Selective surface-enhanced Raman scattering detection of Tabun, VX and Cyclosarin nerve agents using 4-pyridine amide oxime functionalized gold nanopillars

Juhlin, Lars; Mikaelsson, Therese; Hakonen, Aron; Schmidt, Michael Stenbæk; Rindzevicius, Tomas; Boisen, Anja; Käll, Mikael; Andersson, Per Ola

Published in:
Talanta

Link to article, DOI:
10.1016/j.talanta.2020.120721

Publication date:
2020

Document Version
Publisher's PDF, also known as Version of record

Talanta 211 (2020) 120721

Contents lists available at ScienceDirect

Talanta

journal homepage: www.elsevier.com/locate/talanta

Selective surface-enhanced Raman scattering detection of Tabun, VX and Cyclosarin nerve agents using 4-pyridine amide oxime functionalized gold nanopillars

Lars Juhlin[a], Therese Mikaelsson[a], Aron Hakonen[c], Michael Stenbæk Schmidt[d], Tomas Rindzevicius[e], Anja Boisen[e], Mikael Käll[c], Per Ola Andersson[a,b,*]

[a] CBRN Defence and Security, Swedish Defence Research Agency, FOI, SE-90182, Umeå, Sweden
[b] Department of Engineering Sciences, Uppsala University, SE-751 21, Uppsala, Sweden
[c] Department of Physics, Chalmers University of Technology, 412 96, Göteborg, Sweden
[d] Silmeco ApS, 2450 Copenhagen, Denmark
[e] Department of Health Technology, Technical University of Denmark, Ørsteds Plads, 2800 Kgs. Lyngby, Denmark

ARTICLE INFO

Keywords:
Nerve agents
SERS
Indirect detection
Selective binding
Amide oxime
Nanopillars

ABSTRACT

We have earlier demonstrated sensitive detection of low the volatile nerve agents Tabun, Cyclosarin and VX by using handheld Raman instrumentation in conjunction with surface-enhanced Raman scattering (SERS) attained with gold and silver coated Si nanopillar substrates. In the present proof-of-concept study, the gold substrates chemically are functionalized to realize selectivity towards organophosphorus compounds (OPs) with high sensitivity. A potential capturer and reporter molecule, chemical nerve agent antidote, 4-pyridine amide oxime, is evaluated due to its high Raman cross section, high chemical affinity towards gold, and binding specificity to the target substances Tabun, VX and Cyclosarin via the oxime group. Upon selective and covalent binding, the SERS probe undergoes structural changes which are reflected in the spectral SERS responses, making it suitable for indirect monitoring of nerve agents in aqueous solution. With the probe attached to the hotspots of Au-coated Si nanopillars, the SERS signals distinctly discriminate between specific and non-specific analyte binding of Tabun, Cyclosarin and VX down to sub ppm levels. SERS spectrum of 4-PAO is measured after microliter drop coating of aqueous sample solution onto the functionalized substrates and subsequent water evaporation from surfaces. This binding assay is complemented by letting functionalized substrates being immersed into sample solutions 1 h before measuring. Binding specific SERS response decreases in following order: Tabun > VX > Cyclosarin. Overall, the concept looks promising, as expected the candidate probe 4-PAO introduces selectivity to the nanopillar gold substrates without loss of sensitivity.

1. Introduction

Nerve agents (NAs) are highly toxic chemical weapons that bind covalently and irreversible to the essential enzyme acetylcholinesterase (AChE), causing neurotransmission disruption. NAs are therefore lethal by inhalation [1] at low doses. All NAs are prohibited and storage supplies must undergo chemical destruction in accordance to the chemical weapons convention (CWC) [2]. However, in spite of that, NAs have been used in chemical attacks in Japan (1995), Iraq (2004), Syria (2013, 2017) and England (2018). In such situations, it is vital to initiate adequate medical treatment as soon as possible, which in turn motivate development of reliable and rapid in-field detection technologies. This is particularly true for NAs from the G- and V-series, where Tabun (GA), Cyclosarin (GF), and VX, are persistent and have low volatility, making detection based on gas phase analysis less effective. Furthermore, in real world scenarios, these substances are likely to be dispersed in complex matrices. This complicates the detection approach since it requires not only high sensitivity but also a trustworthy selectivity [3,4]. Ruggedized portable instruments for rapid in-field detection of *vaporized* nerve agents based on flame photometry (FP) and ion mobility spectrometry (IMS) [5] have been commercialized. More accurate and general techniques, like GC-MS [5,6] can also work in field conditions, but they require more sample preparation and are overall much more time consuming.

Various fluorescent and colorimetric molecular probes have recently been reported to show both high sensitivity and high selectivity

* Corresponding author. CBRN Defence and Security, Swedish Defence Research Agency, FOI, SE-90182 Umeå, Sweden.
E-mail address: perola.andersson@foi.se (P.O. Andersson).

https://doi.org/10.1016/j.talanta.2020.120721
Received 22 August 2019; Received in revised form 2 January 2020; Accepted 6 January 2020
Available online 08 January 2020

towards NAs and NA simulants, such as organophosphorus compounds (OPs) [7–10]. As an alternative rapid optical analysis technique, Raman scattering, especially surface-enhanced Raman scattering (SERS), offers not only high sensitivity but also spectral richness useful in discrimination among molecules. Raman scattering is a very weak optical process compared to fluorescence, but by letting target molecules attach to nanostructured noble metal surfaces that support surface plasmon resonances, thereby enabling SERS [11], chemical trace analyses become possible. In contrast to normal Raman spectroscopy, SERS analysis does not require high laser powers and competing fluorescence signals are typically quenched due to the proximity of the analytes to the metal surface. Indeed, the last decade has seen encouraging steps towards development of SERS into a powerful and general analysis technique, as demonstrated by applications in environmental analysis [12], e.g. for detection of insecticides and pesticides, medicine [13], bioanalysis [14], agriculture [15], food chemistry [16], authentication [17], anti-counterfeiting [18], forensics [19], security and defence [4,19]. Moreover, portable IR and Raman vibrational spectroscopy instrumentation are today commonly used in field conditions by military and first responders for rapid non-destructive identification of bulk materials. Thus, much speaks for the development of compact affordable SERS sensing devices aimed for rapid trace analysis of nerve agents.

Nerve agents exhibit low intrinsic Raman cross-sections and weak affinity to Au, resulting in relatively high limits-of-detections in SERS, about 1 mg/mL [4,20]. Recently though, lower levels (typically around 1–20 μg/mL) have been reported using bare SERS substrates, that is, without using a particular coupling chemistry that selectively binds the target analyte to the metal surface [21–23]. Unfortunately, in mixed/crude samples, it is very hard to distinguish signals arising from the NA target from those due to background in such a “direct” sensing methodology. This issue was considered in reviews on SERS methods for rapid detection of chemical pesticides, as OPs, abundant in complex matrices [16,24]. One way around the problem is to combine SERS with other analytical techniques, such as extraction and separation procedures, while another strategy is to functionalize the SERS surfaces with an affinity layer, e.g. antibodies, aptamers and molecularly imprinted polymers, to gain specificity towards target compounds and to reduce background signals [16,24]. To avoid time-consuming pre-purification steps, we have evaluated the latter approach, an *indirect* SERS sensing method based on a reporter molecule, pyridine (or pyridyl) amide oxime (4-PAO, Fig. 1) aimed for specific binding to OPs, as GA, GF and VX, dissolved in water solutions. Generally speaking, this approach is encouraged by recent studies on selective sensing of small molecules as hydrogen sulfide [25] and carbon monoxide in living cells [26], pesticides in liquid phase [27], and especially for studies performed on NA simulant as methanephosphonic acid (MPA) [28] and on G-agents [3]. Presently, an indirect sensing methodology is set up that is easy and rapid to use. 4-PAO was chosen since pyridines bind to gold “covalently” via the pyridine nitrogen and are well known for their high SERS activity [29], while oximes (containing the group C═N–OH) is an active moiety in NA antidotes aimed to reactivate AChE to normal function after being inhibited by OP poisoning. The phosphorylated OP-AChE conjugate undergoes a nucleophilic attack by the oxime, which restores the enzyme to the active state and allows nerve impulses to retain normal function. Amide oximes are highly reactive towards electron-deficient centers, such as phosphoryl groups containing good leaving groups. The SERS spectrum of 4-PAO can be expected to change significantly when its oxygen center is bound to the phosphorus atom of NA, since the free carboxamide oxime group is in a planar Z-configuration stabilized by an intramolecular hydrogen bond [30,31]. The N-hydroxyimidamide group also confers good water solubility while retaining high reactivity in a wide pH-range [30,31]. Thus, this compound can be expected to show high reactivity with OP compounds and at the same time display stable and intense SERS signals. Actually, a decade ago, Killops et al. proposed a similar concept using mercaptooximes in aqueous samples as capture molecules for detection of nerve agents, which was characterized by means of NMR, Raman and SER spectroscopy [32].

For SERS measurements, we utilized well known and commercially available SERS substrates composed of flexible gold-coated Si nanopillars fabricated by the mask-free reactive ion etching technique [33,34]. These substrates exhibit interesting adhesion and elasto-capillarity properties highly useful for SERS analysis, as reported elsewhere [21,34]. Upon applying a droplet of the target aqueous solution to the SERS substrate and subsequently letting it dry out, the nanopillars lean together to capture the target substance between the metal-coated pillar ends. The so-formed “hot spot” clusters generate strong electric field-enhancement resulting in Raman surface-enhancement factors up to 10^8 [21,34]. Various analytes in the area of forensics and security have been analyzed the last few years with these substrates, including the nerve agents VX, GA [21] and GF [22], and the explosive picric acid [35], demonstrating excellent performance and sensitivity with both Ag and Au coating in non-functionalized format.

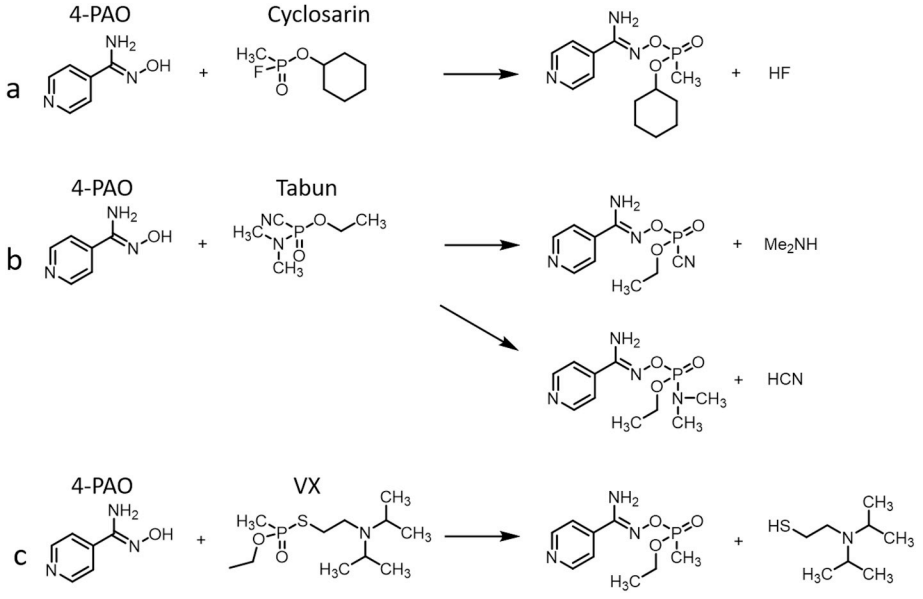

Fig. 1. Reactions in chloroform between probe molecule 4-PAO and GF (a), GA (b) and VX (c), respectively, inferred from NMR data. Similar reaction with the chemical agent simulant, diethyl chlorophosphate (DECP), is shown in the Supplementary Material (Fig. S15) with corresponding normal Raman (Figs. S20–21) and SERS (Figs. S22–23) spectra of the adduct.

2. Materials and methods

2.1. Purity of nerve agent, simulant, and reference substances

The reference substance ethyl methylphosphonic acid (EMPA, CAS 1832-53-7) and chemical simulant diethyl chlorophosphate (DECP, CAS 814-49-3) were of 98 and 97% purity, respectively, and purchased from Sigma Aldrich.

^{1}H and ^{31}P NMR spectra of Cyclosarin, Tabun and VX are shown in the Supplementary Materials together with GC-MS chromatograms. The NMR analyses were performed with a Bruker Avance III HD 500 spectrometer equipped with a double resonance broadband cryoprobe.

Cyclosarin, Tabun, and VX were diluted with dichloromethane to a concentration of 50 ppm and analyzed with GC/MS using electron ionization. The purity of the compounds was calculated from the relative top-area in respectively total-ion chromatogram and found to be 98.1, 92.7 and 87.4% for GA, VX and GF, respectively. The response of the impurities relative the main component may vary, but as they are closely related to the main components, the accuracy in the main component is estimated to be good, particularly for the compounds with purity over 90%. Chemical analyses using GC-MS only reveal volatile compounds and some degradation products, such as phosphonic acids, that require derivatization in order to be detectable with GC-MS, were therefore not performed here.

2.2. Synthesis of probe molecule 4-PAO and adducts

Pyridine (or pyridyl) amide oxime, 4-PAO, was synthesized as follows: A C18 analytical column (50 × 2.1 mm) was eluted with a mixture of acetonitrile, water and 0.1% formic acid at a flow rate of 1.5 mL/s. A linear gradient was first used, starting with 95% water and ending with 98% acetonitrile after 2 min, followed by isocratic flow. 4-cyanopyridine, 2.08 g, was dissolved in 25 mL 2-propanol. A solution of 1.39 g hydroxylamine hydrochloride in 5 mL 4 M sodium hydroxide was slowly added to the stirred solution during 15 min. The final solution was then stirred at room temperature (RT) overnight. The precipitate was filtered off and recrystallized from 2-propanol. All compounds were analyzed with a Waters 2998 HPLC system equipped with a PDA detector and an Acouity QDa Mass Detector. The synthetic routes of expected adducts are described in Supplementary Material.

2.3. Reactions in solution phase measured with NMR

The nerve agents Tabun, Cyclosarin, VX and the nerve agent simulant DECP were allowed to react with 4-PAO in $CDCl_3$ containing 10% CD_3CN at 50 °C. To trace the reactions over time, NMR spectra were collected after 1 and 3 days and finally after 30 days at RT for all substances.

2.4. Raman instrumentations

A confocal Raman microscope (LabRam HR800UV, Horiba Jobin Yvon) was used to study SERS signatures from functionalized substrates spiked with Tabun (GA), VX, Cyclosarin (GF), and the control substance ethyl methylphosphonic acid (EMPA). In addition, a handheld Raman instrument (First Defender RMX) was applied for the GA and EMPA samples. The excitation laser wavelength was in both cases 785 nm and the power on the SERS substrates were approximately 10 mW using the confocal Raman microscope (CRM) and 110 mW with the portable instrument. The CRM is equipped with two mirrors attached to piezo-crystals in the light path, which allows deflection of the laser beam trough the objective and illumination of a larger sample spot area. Here, a 10× objective (NA = 0.25) was used and a spot size of 50 × 50 μm was probed to generate spectra in the range of 200–2500 cm^{-1}. The Raman scattering light is dispersed by a 300 grooves/mm grating in a f = 80 cm spectrograph and detected by an Andor Newton thermoelectrically cooled (−65 °C) EM-CCD camera. The confocal hole was set to 500 μm, and the overall system response was taken into account by correcting measured spectra relative those performed on a NIST standard reference material (SRM2241). In the case of the portable Raman instrument, the scattered light was collected in a back scattering geometry at a distance of ~5 mm and using a laser spot diameter of the order 100–150 μm.

2.5. SERS substrates and methodology

Gold covered nanostructured silicon (Si) nanopillar SERS substrates were fabricated using mask-less lithography process [33,34]. In brief, the SERS substrate fabrication process involves two steps: (i) Si NP's are obtained via mask-less reactive ion etching (RIE) of silicon using a SF_6 and O_2 gas mixture, and (ii) a 200 nm thick Au metal film is deposited using electron beam evaporation. The resulting SERS substrates contain ~500 nm in height Au-capped NP structures (~18 pillars/μm^2), see Fig. S14 in the Supplementary Material. The Au caps are approximately ellipsoidal in shape, and the Au cap dimensions are the following: height ≈300 nm, width ≈100 nm. The Au NP structures were additionally coated with 4-PAO reporter molecules dissolved in milliQ water. Two microliters of 100 ppm 4-PAO solution was first pipetted onto the substrate, after which the water was evaporated. Aliquots of 2 μL sample solution, with a zero concentration represented by pure water, were then pipetted on the 4-PAO spot. The SERS measurement started after a few minutes, when the water had evaporated. Five different regions of the functionalized spot were analyzed at each sample concentration. Spectral data represent an average of five replicates. The spectral acquisition time was 20 s (2 × 10 s) and 2 s for the CRM and the handheld device, respectively.

In SERS immersion experiments, the functionalized substrates were kept in a solution of the chemical agent for 60 min. The substrates were then rinsed with pure milliQ water before SERS measurements. Water (pH 6.5) from lake was first filtrated using 5 μm pore size Nylon filters (Titan) and was used in immersion tests with VX.

All samples were prepared in immediate conjunction to the SERS measurements to avoid degradation of the NAs due to hydrolyzing. The degradation of Cyclosarine (GF) in water was analyzed using ^{31}P NMR. The % degradation was calculated by comparison of integrated peaks from GF and the degradation product cyclohexyl methylphosphonic acid (Table S1).

Min-max normalization to the peak centred at 1605 cm^{-1} was done. This band corresponds to C=C stretching mode of pyridine ring and is assumed to be insensitive to binding of analytes through the N–O(H) oxime moiety of the probe molecule 4-PAO (Fig. 1).

The limit of detection (LOD) was estimated from the standard deviation (sr) of five replicate measurements on the zero level (blank) signal for a particular peak (max response peak or best selectivity, here 945 and 1220 cm^{-1} peaks for VX and Tabun, respectively) and the slope (k) between zero and lowest measured level according to standard approximation LOD = 3sr/k [36]. Relative standard deviations (RSD) were calculated for the measurements corresponding to the binding curves of GA and VX, and are listed in Supplementary Table S3. Statistical validated analysis on reproducibility among substrate performances was out of the scope in this proof-of-concept study.

2.6. Langmuir equilibrium adsorption isotherms

The oxime group of 4-PAO can be expected to react with the nerve agent (NA) to yield the adduct NA-PAO. Although the conditions for the Langmuir isotherm not are fulfilled, it is qualitatively applied here to describe the concentration dependence and it is assumed to following the modified form (saturation binding curve):

$$[NA - PAO] = \frac{B_{max} \times [NA]}{K_d + [NA]} \quad (1)$$

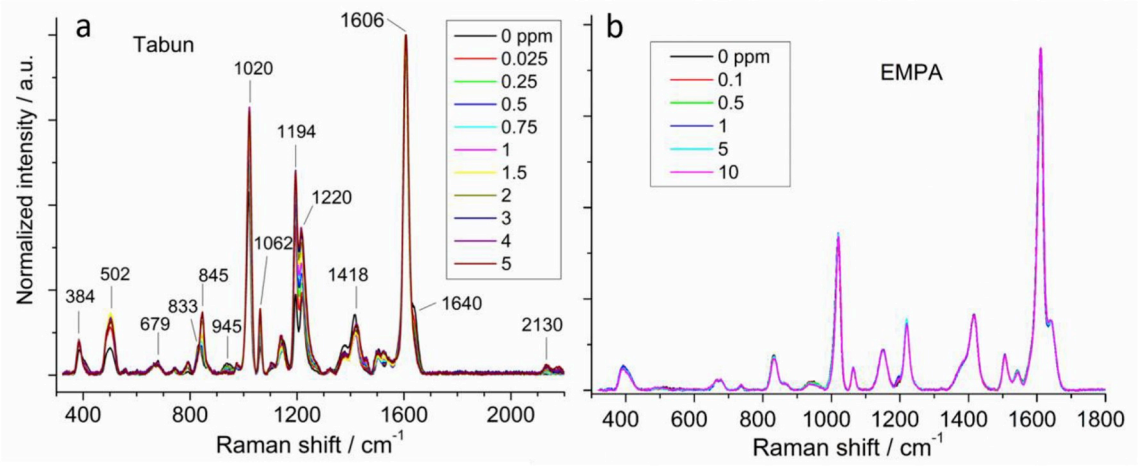

Fig. 2. Normalized SERS average spectra of 100 ppm 4-PAO measured using handheld Raman instrumentation. Aliquots of 2 μL Tabun (a) and EMPA (b) solutions were titrated on SERS substrates functionalized with 4-PAO.

where B_{max} is the maximal number of binding sites $[NA-PAO]_{max}$ and K_d is the dissociation constant. The spectral change (intensity or waveband shift, denoted ΔI) of specific peaks at chemical equilibrium is assumed to be proportional to the number of occupied sites, i.e. $[NA-PAO] = const \times \Delta I$ and $[NA-PAO]_{max} = const \times \Delta I_{max}$. This gives

$$\Delta I([NA]) = \frac{\Delta I_{max} \times [NA]}{K_d + [NA]}, \quad (2)$$

where [NA] (= $[NA]_{free}$) is approximated with the bulk concentration of NA. By plotting ΔI as a function of [NA] and fitting the data with Eq. (2), one can then estimate K_d (μM) and binding strengths.

3. Results and discussion

3.1. NMR analyses of NA reactions with 4-PAO in solvent

The reactivity of 4-PAO towards GA, GF and VX, respectively, in chloroform, was first confirmed through NMR experiments (Fig. 1, Figs. S16–S19). The reaction between 4-PAO and Cyclosarin (GF) resulted in formation of a new O–P bond and displacement of fluorine, as expected, yielding a methylphosphonate and hydrogenfluoride as products (Fig. 1a). The reaction with Tabun (GA) may results in two different products (Fig. 1b). The NMR data show that the P–CN bond breaks after O–P bond formation, resulting in a phosphoramidate and hydrogencyanide. In the reaction with VX, the cleavage occurs between P and S, giving a methylphosphonate and 2-(diisopropylamino)-etanthiol (Fig. 1c).

3.2. Normal Raman spectroscopy of synthesized adducts

Normal Raman scattering spectra were measured for 4-PAO and corresponding adducts (4-PAO-X), in order to characterize the spectral properties of the chemical probe (Supplementary Material Figs. S20–S21). The spectral region between 900 and 1800 cm^{-1} is dominated by vibrational modes originating from PAO moiety of the adduct while at lower frequencies other bands show up compared to free 4-PAO. Spectral changes of relative intensities and band frequencies in region 800–1800 cm^{-1} were found to be most useful when analyzing the indirect SERS sensing results. Notable, the peak of CN group normally seen about 2100–2200 cm^{-1} for GA is absent in Raman spectrum of GA-adduct (Figs. S20–21A).

3.3. SERS spectra of chemical probe attached to gold nanopillars

GA, GF and VX decompose in water solutions due to hydrolysis and the degradation rates are dependent on pH and temperature. In current state, RT (~22 °C) and neutral pH, the rate of decomposition corresponds to half-life times about 8 h for Tabun and many days for VX [37]. With ^{31}P NMR we have studied the hydrolyzing of Cyclosarin in D_2O (20 mM) and estimated the half-life time to be 16 h (Table S1). Thus, when the fresh spiked water samples are analyzed with SERS the NAs are primarily intact, and besides, the formed degradation products, as for example control substance EMPA, exhibit low affinity to both 4-PAO and gold surface, and hence do not produce any interfering SERS signals.

SERS spectra of synthesized adducts (4-PAO-X) were only obtained for DECP adduct (Figs. S22–23), since the adducts of GA, GF and VX precipitate on the hydrophobic SERS surfaces making it impossible to measure any relevant SER spectra. The result from DECP adduct indicates that spectral SERS discrimination is possible to attain due to specific binding of the NAs to the chemical probe 4-PAO. Upon chemical functionalization, 4-PAO binds to the nanostructured gold surface through the pyridine, resulting in a Au–N bond characterized by a SERS band at 249 cm^{-1} [38]. As expected, this band is missing from the normal Raman spectrum of 4-PAO (Fig. S20). When NAs in aqueous solutions are added and allowed to bind to the oxime group of 4-PAO, structural changes reflected in the SERS spectra of 4-PAO occur. These changes were reproducible and most evident for GA and least pronounced for GF. Results from VX drop coating experiments are shown in Supplementary Material (Fig. S33). However, when functionalized substrates were immersed in sample solutions of GF and VX larger spectral responses, similar to those of GA in drop-and-dry sampling, showed up, as further discussed below. All vibrational bands in the fingerprint region originate from the chemical probe, 4-PAO (Fig. 2), with exception for weak bands at 2100-2200 cm^{-1} upon GA titration (Fig. 2a). The control substance ethyl methylphosphonic acid (EMPA) was also examined in similar concentration ranges but no systematic spectral changes were found to occur (Figs. 2b and S25). Indeed, this compound is not expected to react with the oxime group, i.e. the N–OH group of 4-PAO stays intact.

Band assignments and responses are summarized in Table S2 in the Supplementary Material. In short, prominent peaks of 4-PAO occur at 1640 (C═N stretch), 1605 (C═C stretch), 1420 (pyridine ring stretch), 1220 (C–C stretch, CH def), 1194 (CH def, CN def), 1146 (CH def), 1062 (CH def), 1020 (pyridine ring stretch), and 833 cm^{-1} (C–N and NH stretch) [39,40]. The latter peak is not seen in the SERS spectrum of the related compound 4-**P**yridin**A**ldoxim (4-PA), that is missing the NH_2

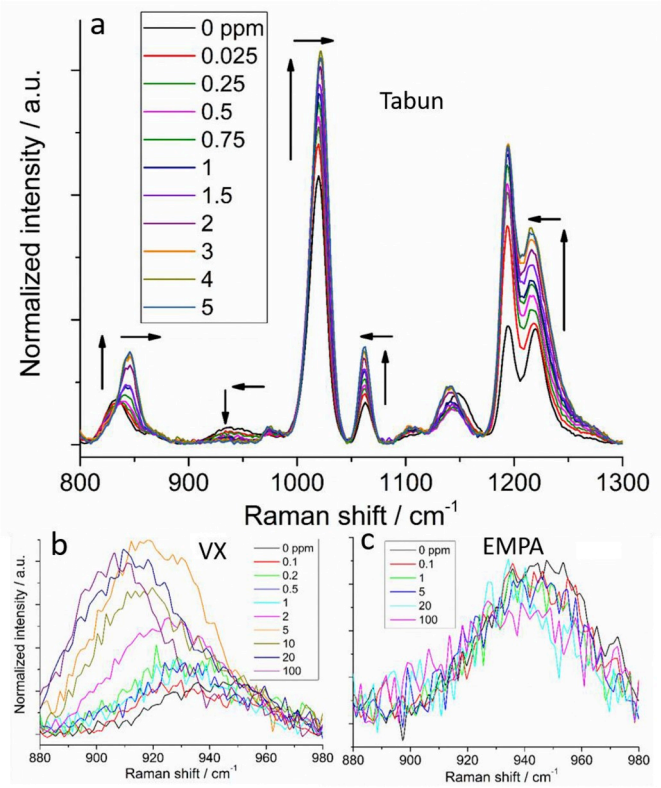

Fig. 3. Normalized SERS average spectra of 100 ppm 4-PAO. Aliquots of 2 μL Tabun (a), VX (b) and EMPA (c) solutions are titrated on SERS substrates functionalized with 4-PAO. Handheld Raman instrumentation is used for Tabun and a Raman microscope for VX and EMPA. Only the N–O(-X) stretching bands of 4-PAO are shown in case of VX and EMPA. In b) and c) full spectra are first baseline corrected and then cut between 880 and 980 cm^{-1}, and subsequently baseline corrected a second time.

group of the oxime moiety (Fig. S24), hence this band likely dominates by vibrational modes of the C–NH_2 group. Peaks that systematically change upon GA titration are located at 1220, 1063, 1020 and 833 cm^{-1}. Common for all substances analyzed, including EMPA, the two bands seen at 1194 and 502 (not assigned) cm^{-1} were changed without systematic trend correlated to the concentration (see also Figs. S25–S27). They also fluctuate in intensity over time, which currently not is understood, and out of the scope for further investigations in this conceptual study. To speculate these vibrational modes of 4-PAO are more sensitive to water interactions, which may vary over time when 4-PAO is anchored to nanopillars. For GA the peak at 833 cm^{-1} increases in relative intensity by approximately a factor of two and shifts gradually to 846 cm^{-1} (Figs. 3a and S27). The 1220 peak is downshifted to 1215 cm^{-1} and exhibits a concomitant twofold intensity increase (Figs. 3a and S27). The N–O(H) stretching mode of oximes is known to produce a weak plateau band around 945 cm^{-1} [39,40], which herein downshifts when the hydrogen exchanges to a NA adduct. In reaction with VX, this band is approximately doubled in intensity (Figs. 3b and S33), which also is recorded for the DECP adduct (Figs. S22–23A), while for GA it is diminished (Fig. 3a, Fig. S27). It can not be excluded that the intense SERS peak of VX centred at 890-895 cm^{-1} [3,21], assigned to OPC and/or CCN stretch vibrational mode of VX, also contributes to the spectral responses of this band, especially at higher VX concentrations. However, since spectral responses of VX in immersion experiments (section 3.5), agree with those of GA obtained in titration experiments, though less pronounced, and similar shift of the DECP adduct, it is reasonable to suggest that the main part of this down shift from –945 to –905 cm^{-1} originates from specific binding between 4-PAO and VX (Fig 3b, Fig. S33). GA and VX seem to influence certain vibrational modes of 4-PAO in different ways, and thereby they likely can be separated in more detailed spectral analyses for example based on multivariate data modelling. Moreover, in the case of GA at higher concentrations (> 1 ppm), weak bands at 2135 and at 2180 (very weak) cm^{-1} increase linearly with concentration (Figs. 2a, S30 and S32), a result that agrees with earlier observations of Tabun [21]. Here they are supposed to originate from non-specifically adsorbed Tabun and/or HCN attached to the bare Au surface. Worth to mention here is that chemical compounds containing cyano-groups having good electrophilic property can react with 4-PAO and affect the SERS detection. Besides, it is likely that all nerve agents containing O-alkylated phosphoryl groups show similar SERS signals.

The reactions in Fig. 1 are supposed to be pH-dependent. Herein all experiments were performed under neutral conditions. To speculate, an increase of pH to 12 may increase the reaction rate constant about 100 times according to Prokop'eva et al. [30], but on the other hand, it may also give rise to a considerable increase in the rate of hydrolysis of NAs, and also affect the stability of the oxime-NAs adduct [3]. Another possible way to increase the reactivity of amidoximes is by full methylation of the amino-group. This causes the amidoxime to take an E-form isomer because of loss of an internal hydrogen bond, which occurs between the oxygen atom in the oxime and a hydrogen in the amino group. This can enhance the reaction rate up to hundred times [30]. Otherwise, a change in nucleophile site from oxygen to nitrogen, as for hydrazones, may alternatively be a proper way to increase the rate.

3.4. Saturation binding curves for 4-PAO reaction with GA and VX

From GA titration between 0.02 and 5 ppm (vol/vol), saturation curves were obtained using intensity changes of the three peaks at 846 (Figs. S29, S31), 1020 (Fig. S29) and 1220 (Fig. 4a) cm^{-1}, whilst for VX a corresponding curve was generated by studying the spectral shift of the band at 945 cm^{-1} in the concentration range between 0.1 and 100 ppm (Fig. 4b). No saturation curve was obtained for GF. The apparent lower spectral response upon drop coating of GF originates probably not from its lower sample purity. Instead, the structural discrepancies likely have impact on the specific interactions and kinetics differently, resulting in slower reaction rate and a longer reaction time to reach chemical equilibrium state for GF compared to GA. However, due to the convenience and the small sample amounts needed, the drop-and-dry approach was still used to evaluate the concentration dependence for these extremely toxic NA samples. We assume that the number of occupied sites (PAO-adduct complexes) are proportional to the change of SERS signal upon titration and thus plot the intensity at 1220 cm^{-1} of GA versus concentration in Fig. 4a. The trend is found to be qualitatively and surprisingly well described by the Langmuir equilibrium adsorption model (Eq. (2)), assuming one binding site (Eq. (2)). Even if the state of chemical equilibrium, in the case of pipetting the solution followed by evaporation, is not clear to us as above mentioned, we acknowledge the fact that the Langmuir isotherm seems to describe the overall concentration dependence very well. The binding strength is estimated from the dissociation constant K_d –10 μM (thus similar to weak affinity of protein-ligand binding).

Results from other bands of GA, 846 and 1020 cm^{-1} (Figs. S29 and S31) follow similar trends. For VX, the peak maximum of NO-X band shifts from ~945 to 905 cm^{-1} when concentration goes from 0.1 to 100 ppm. A model of two binding sites was applied to attain sufficiently good fitting (R^2 = 0.99), resulting in two K_d;s of 0.1 and 24 μM (Fig. 4b). A wider dynamic range is obtained for VX relative to GA, and VX saturates the functionalized surface at higher concentration than GA. Limit of detection (LOD) is estimated from these responses to be 0.2 μM for GA and 0.4 μM for VX. These limits are roughly the same as the best ones previously reported in other studies on bare gold SERS substrates, i.e. without selectivity [4,21,22,41]. Values of RSD are given in Table S3 and are found to vary between 1 and 6% for GA and 0.2–0.9% for VX.

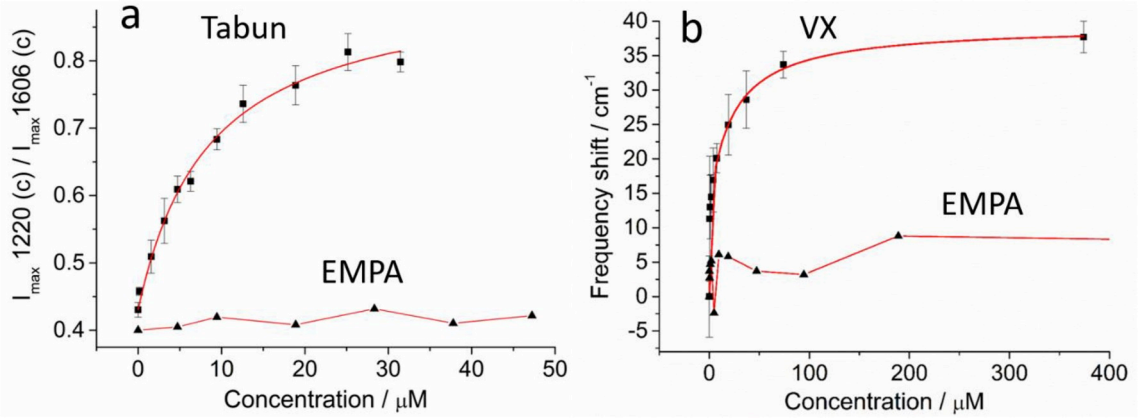

Fig. 4. Adsorption isotherms for Tabun and VX obtained in drop-and-dry experiments. Intensity rise at 1220 cm^{-1} for Tabun is fitted with one binding site approximation (K_d = 8.5 ± 0.91 μM, R^2 = 0.99) whereas spectral shift at 945 cm^{-1} for VX needs two binding sites approximation (K_{d1} = 0.09 ± 0.03 μM, K_{d2} = 23.9 ± 2.44 μM R^2 = 0.99). No spectral trend was seen for control substance EMPA.

3.5. SERS spectra of GA, VX, GF and EMPA after substrates being immersed in solution

The binding kinetics are not examined herein, but due to structural discrepancies [42] it is likely to vary among the analytes. When SERS substrates are immersed in solution (1 h) chemical equilibrium is likely to occur. In such experiments both VX and GF induce larger spectral responses on the SERS probe than in drop-and-dry experiments (Fig. 5 and Figs. S33–S39). Fig. 5 displays two vibrational bands at 840 and 945 cm^{-1}, both belonging to the oxime group of 4-PAO. Immersions in pure water (MQ), in lake water and in EMPA solution, respectively, have no impact (due to non-specific binding) on the vibrational modes of 4-PAO, whereas in a mixture of GA (5 ppm) and EMPA a substantial change was revealed (Figs. 5a, S34-S35). A similar spectral pattern was seen for GF in MilliQ water (Figs. 5c, S38-S39). When VX was dissolved (20 ppm) in impure lake water a major shift of NO-X peak was found, corresponding to 100 ppm in drop-and-dry experiment (Figs. 3b and 4b). For VX additional bands, e.g. at 1020 and 1220 cm^{-1}, were here also realized (Figs. S36–S37) according to results from GA titration. The longer incubation times seem to facilitate the binding kinetics to reach thermodynamic equilibrium. GF follows this description as well, with spectral modifications at several vibrational bands, i.e. at 840, 1020, 1063 and 1217 cm^{-1} (Figs. 5c, S38-S39).

Finally, the bond between 4-PAO, via the lone-pair of the pyridine nitrogen (electrophile), and the gold surface was found to be stable up to incubation times of at least 6 h, resulting in reliable reproducible 4-PAO SERS spectra. Nevertheless, thiol bonds are likely even stronger and therefore probably a better choice to link the chemical probes to SERS substrate [32]. This was recently applied in a work on detection of lung-cancer biomarkers based on a related indirect and selective SERS methodology [43].

4. Conclusions

In conclusion, this study demonstrates the promising concept of using the oxime derivative 4-PAO (pyridine (or pyridyl) amide oxime) chemically bound to nanopillar gold surfaces for sensitive and selective SERS trace detection of nerve agents Tabun, Cyclosarin and VX. Estimated detection limits 0.2 μM for GA and 0.4 μM for VX are roughly the same as the best ones previously reported in other studies on bare gold SERS substrates without selectivity. As hypothesized, the SERS vibrational bands of 4-PAO change significantly when its oxygen center binds to the phosphorus atom of the NAs. The spectral richness of the SERS data is well suited for use in statistical analyses, as in pattern recognition models, to support discriminations among targets. The next step is to implement a systematic optimization methodology to find the best chemical probes. SERS flow thru experiments could be an effective complement to drop-and-dry and immersion experiments. This would enable fundamental in-situ studies to gain information about binding kinetics and strengths, environmental effects, pH dependence, diffusion rates, temperature effects and thermodynamic parameters.

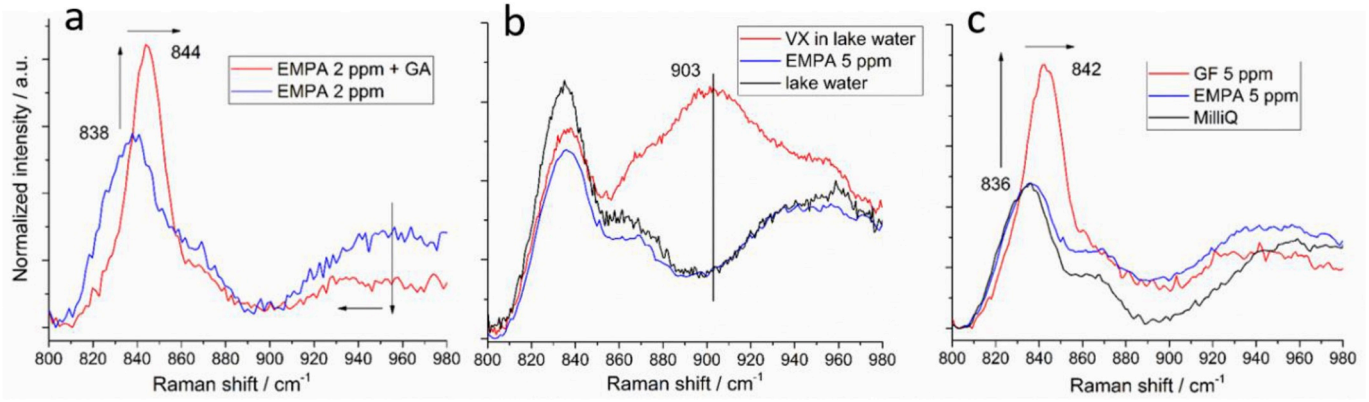

Fig. 5. SERS spectra of 4-PAO functionalized substrates immersed (1 h) in solutions are depicted. a) EMPA (blue) and mixture of EMPA and GA (red) in MQ water. b) Lake water (black), EMPA in MQ water (blue), and VX dissolved in lake water (red). c) Pure MQ water (black), EMPA in MQ water (blue) and GF in MQ water (red). (For interpretation of the references to color in this figure legend, the reader is referred to the Web version of this article.)

Declaration of competing interest

T. Rindzevicius, A. Boisen and M. S. Schmidt are co-founders of the Silmeco ApS company.

Acknowledgements

This work was funded by the Swedish Department of Defence, Project nos. 410-A403218 and I490407. The research was also financially supported by the IDUN Center of Excellence, funded by the Danish National Research Foundation (Grant no. DNRF122) and the Villum Fonden (Grant No. 9301), and the Swedish Foundation for Strategic Research (Grant No. RMA 0037).

Appendix A. Supplementary data

Supplementary data to this article can be found online at https://doi.org/10.1016/j.talanta.2020.120721.

References

[1] P. Taylor, Z. Radic, The Cholinesterases - from genes to proteins, Annu. Rev. Pharmacol. Toxicol. 34 (1994) 281–320.
[2] Organisation for the prohibition of chemical weapons - OPCW, https://www.opcw.org/our-work/demilitarisation/destruction-of-chemical-weapons/ , Accessed date: 20 August 2019.
[3] J.F. Wu, Y.J. Zhu, J. Gao, J. Chen, J.L. Feng, L. Guo, J.W. Xie, A simple and sensitive surface-enhanced Raman spectroscopic discriminative detection of organophosphorous nerve agents, Anal. Bioanal. Chem. 409 (2017) 1–9.
[4] A. Hakonen, P.O. Andersson, M. Stenbaek Schmidt, T. Rindzevicius, M. Käll, Explosive and chemical threat detection by surface-enhanced Raman scattering: a review, Anal. Chim. Acta 893 (2015) 1–13.
[5] WMD Detector Selector, https://www.wmddetectorselector.army.mil/ , Accessed date: 20 August 2019.
[6] R. Sferopoulos, A review of chemical warfare agent (CWA) detector technologiesand commercial-off-the-shelf items, in: ADOD Defence (Ed.), DSTO Defence Science and Technology Organisation, 506 Lorimer St. Fishermans Bend, Victoria 3207, Australia, 2009.
[7] B.D. de Grenu, D. Moreno, T. Torroba, A. Berg, J. Gunnars, T. Nilsson, R. Nyman, M. Persson, J. Pettersson, I. Eklind, P. Wasterby, Fluorescent discrimination between traces of chemical warfare agents and their mimics, J. Am. Chem. Soc. 136 (2014) 4125–4128.
[8] Y. Kim, Y.J. Jang, D. Lee, B.S. Kim, D.G. Churchill, Real nerve agent study assessing pyridyl reactivity: selective fluorogenic and colorimetric detection of Soman and simulant, Sens. Actuators B Chem. 238 (2017) 145–149.
[9] Y. Kim, Y.J. Jang, S.V. Mulay, T.T.T. Nguyen, D.G. Churchill, Fluorescent sensing of a nerve agent simulant with dual emission over wide pH range in aqueous solution, Chem. Eur J. 23 (2017) 785–790.
[10] Y.J. Jang, O.G. Tsay, D.P. Murale, J.A. Jeong, A. Segev, D.G. Churchill, Novel and selective detection of Tabun mimics, Chem. Commun. 50 (2014) 7531–7534.
[11] M. Fleischmann, P.J. Hendra, A.J. McQuillan, Raman spectra of pyridine adsorbed at a silver electrode, Chem. Phys. Lett. 26 (1974) 163–166.
[12] H. Wei, S.M.H. Abtahi, P.J. Vikesland, Plasmonic colorimetric and SERS sensors for environmental analysis, Environ. Sci. Nano. 2 (2015) 120–135.
[13] S.S. Sinha, S. Jones, A. Pramanik, P.C. Ray, Nanoarchitecture based SERS for biomolecular fingerprinting and label-free disease markers diagnosis, Acc. Chem. Res. 49 (2016) 2725–2735.
[14] C. Zong, M.X. Xu, L.J. Xu, T. Wei, X. Ma, X.S. Zheng, R. Hu, B. Ren, Surface-enhanced Raman spectroscopy for bioanalysis: reliability and challenges, Chem. Rev. 118 (2018) 4946–4980.
[15] D.A. Jency, M. Umadevi, G.V. Sathe, SERS detection of polychlorinated biphenyls using beta-cyclodextrin functionalized gold nanoparticles on agriculture land soil, J. Raman Spectrosc. 46 (2015) 377–383.
[16] M.L. Xu, Y. Gao, X.X. Han, B. Zhao, Detection of pesticide residues in food using surface-enhanced Raman spectroscopy: a review, J. Agric. Food Chem. 65 (2017) 6719–6726.
[17] D.Y. Lv, Y. Cao, Z.Y. Lou, S.J. Li, X.F. Chen, Y.F. Chai, F. Lu, Rapid on-site detection of ephedrine and its analogues used as adulterants in slimming dietary supplements by TLC-SERS, Anal. Bioanal. Chem. 407 (2015) 1313–1325.
[18] K.J. Si, D. Sikdar, L.W. Yap, J.K.K. Foo, P.Z. Guo, Q.Q. Shi, M. Premaratne, W.L. Cheng, Dual-coded plasmene nanosheets as next-generation anticounterfeit security labels, Adv. Opt. Mater. 3 (12) (2015) 1710–1717.
[19] C. Muehlethaler, M. Leona, J.R. Lombardi, Review of surface enhanced Raman scattering applications in forensic science, Anal. Chem. 88 (2016) 152–169.
[20] S. Farquharson, F.E. Inscore, S. Christesen, Detecting chemical agents and their hydrolysis products in water, Book: Surface-Enhanced Raman Scattering: Physics and Applications vol 103, Springer, Berlin, Heidelberg, 2006, pp. 447–460.
[21] A. Hakonen, T. Rindzevicius, M. Stenbaek Schmidt, P.O. Andersson, L. Juhlin, M. Svedendahl, A. Boisen, M. Kall, Detection of nerve gases using surface-enhanced Raman scattering substrates with high droplet adhesion, Nanoscale 8 (2016) 1305–1308.
[22] A. Hakonen, K. Wu, M. Stenbaek Schmidt, P.O. Andersson, A. Boisen, T. Rindzevicius, Detecting forensic substances using commercially available SERS substrates and handheld Raman spectrometers, Talanta 50 (2018) 649–652.
[23] M. Lafuente, I. Pellejero, V. Sebastian, M.A. Urbiztondo, R. Mallada, M.P. Pina, J. Santamaria, Highly sensitive SERS quantification of organophosphorous chemical warfare agents: a major step towards the real time sensing in the gas phase, Sens. Actuators B Chem. 267 (2018) 457–466.
[24] S.T.R. Pang, T.X. Yang, L.L. He, Review of surface enhanced Raman spectroscopic (SERS) detection of synthetic chemical pesticides, Trac. Trends Anal. Chem. 85 (2016) 73–82.
[25] D.W. Li, L.L. Qu, K. Hu, Y.T. Long, H. Tian, Monitoring of endogenous hydrogen sulfide in living cells using surface-enhanced Raman scattering, Angew. Chem. 54 (2015) 12758–12761.
[26] Y. Cao, D.W. Li, L.J. Zhao, X.Y. Liu, X.M. Cao, Y.T. Long, Highly selective detection of carbon monoxide in living cells by palladacycle carbonylation-based surface enhanced Raman spectroscopy nanosensors, Anal. Chem. 87 (2015) 9696–9701.
[27] X.Z. Li, T.Y. Yang, Y.T. Song, J.H. Zhu, D.L. Wang, W. Li, Surface-enhanced Raman spectroscopy (SERS)-based immunochromatographic assay (ICA) for the simultaneous detection of two pyrethroid pesticides, Sens. Actuators B Chem. 283 (2019) 230–238.
[28] Q. Zhao, G.Q. Liu, H.W. Zhang, F. Zhou, Y. Li, W.P. Cai, SERS-based ultrasensitive detection of organophosphorus nerve agents via substrate's surface modification, J. Hazard Mater. 324 (2017) 194–202.
[29] M.G. Albrecht, J.A. Creighton, Anomalously intense Raman-spectra of pyridine at a silver electrode, J. Am. Chem. Soc. 99 (1977) 5215–5217.
[30] T.M. Prokop'eva, Y.S. Simanenko, E.A. Karpichev, V. Savelova, A.F. Popov, O-nucleophilic features of amidoximes in acyl group transfer reactions, Russ. J. Org. Chem. 40 (2004) 1617–1629.
[31] Y.S. Simanenko, T.M. Prokop'eva, I.A. Belousova, A.F. Popov, E.A. Karpichev, Amidoximes as effective acceptors of acyl group, Theor. Exp. Chem. 37 (2001) 288–295.
[32] K.L. Killops, R.A. Fry, W.R. Creasy, H.D. Durst, J.A. Guicheteau, Mercapto-oximes as capture molecules for detection of nerve agents using surface-enhanced Raman spectroscopy, Edgewood Chem. Biol. Cent., U.S. Army Res., Dev. Eng. Command. (2009) 1–15.
[33] M. Stenbaek Schmidt, J. Hubner, A. Boisen, Large area fabrication of leaning silicon nanopillars for surface enhanced Raman spectroscopy, Adv. Mater. 24 (2012) OP11–OP18.
[34] K. Wu, T. Rindzevicius, M. Stenbaek Schmidt, K.B. Mogensen, A. Hakonen, A. Boisen, Wafer-scale leaning silver nanopillars for molecular detection at ultra-low concentrations, J. Phys. Chem. C 119 (4) (2015) 2053–2062.
[35] A. Hakonen, F.C. Wang, P.O. Andersson, H. Wingfors, T. Rindzevicius, M. Stenbaek Schmidt, V.R. Soma, S.C. Xu, Y.Q. Li, A. Boisen, H.A. Wu, Hand-held femtogram detection of hazardous picric acid with hydrophobic Ag nanopillar SERS substrates and mechanism of elasto-capillarity, ACS Sens. 2 (2017) 198–202.
[36] A. Hakonen, Plasmon enhancement and surface wave quenching for phase ratiometry in coextraction-based fluorosensors, Anal. Chem. 81 (2009) 4555–4559.
[37] K. Kim, O.G. Tsay, D.A. Atwood, D.G. Churchill, Destruction and detection of chemical warfare agents, Chem. Rev. 111 (2011) 5345–5403.
[38] D.Y. Wu, M. Hayashi, C.H. Chang, K.K. Liang, S.H. Lin, Bonding interaction, low-lying states and excited charge- transfer states of pyridine-metal clusters: pyridine-M-n (M = Cu, Ag, Au; n = 2-4), J. Chem. Phys. 118 (2003) 4073–4085.
[39] G. Socrates, Infrared and Raman Characteristic Group Frequencies, third ed., Johns Wiley & Sons, Ltd, Chichester, 2001.
[40] S. Jeyavijayan, M. Arivazhagan, FTIR, FT-Raman spectra and DFT analysis of m-nitrobenzaldehyde oxime, Indian J. Pure Appl. Phys. 50 (2012) 623–632.
[41] S. Farquharson, A. Gift, P. Maksymiuk, F. Inscore, Surface-enhanced Raman spectra of VX and its hydrolysis products, Appl. Spectrosc. 59 (2005) 654–660.
[42] A. Tripathi, E.D. Emmons, N.D. Kline, S.D. Christesen, A.W. Fountain, J.A. Guicheteau, Molecular structure and solvent factors influencing SERS on planar gold substrates, J. Phys. Chem. C 122 (2018) 10205–10216.
[43] X.Z. Qiao, B.S. Su, C. Liu, Q. Song, D. Luo, G. Mo, T. Wang, Selective surface enhanced Raman scattering for quantitative detection of lung cancer biomarkers in superparticle@MOF structure, Adv. Mater. 30 (2018) 1702275.